Title	First-principles investigation of transport properties through longitudinal unzipped carbon nanotubes
Author(s)	Wang, B; Wang, J
Citation	Physical Review B: Condensed Matter and Materials Physics, 2010, v. 81 n. 4 article no. 045425
Issued Date	2010
URL	http://hdl.handle.net/10722/81074
Rights	Physical Review B: Condensed Matter and Materials Physics. Copyright © American Physical Society.

First-principles investigation of transport properties through longitudinal unzipped carbon nanotubes

Bin Wang and Jian Wang*
Department of Physics and The Center of Theoretical and Computational Physics, The University of Hong Kong, Pokfulam Road, Hong Kong, China

(Received 23 June 2009; revised manuscript received 21 November 2009; published 25 January 2010)

We report a first-principles investigation of transport through longitudinal unzipped carbon nanotube based devices. The graphene nanoribbons can be obtained experimentally by unzipping carbon nanotubes in the longitudinal direction. The basic component of our devices is partially unzipped carbon nanotube that consists of graphene nanoribbons and carbon nanotubes as leads. When the edges of graphene are saturated by hydrogen atoms, the system has finite magnetic moment and hence the transport is spin polarized. Our results show that as the Fermi energy is varied the system can change from an insulator to a spin-down half metal, an insulator again, and finally a spin-up half metal. Hence a spin-filter device can be designed from this kind of systems.

DOI: 10.1103/PhysRevB.81.045425 PACS number(s): 72.80.Ey, 73.40.−c, 73.63.−b

I. INTRODUCTION

Since the experimental realization of free-standing graphene,[1] it has been an exciting arena for material science and condensed-matter physics. Graphene consists of one atomic layer of carbon atoms in honeycomb lattice. A remarkable property of graphene is that it behaves like massless Dirac fermions where charge carriers mimic relativistic particles. Investigation of graphene has focused on the quantum-Hall effect,[2–8] spin-dependent transport,[9–12] *p-n* junctions,[13–15] spin qubits,[16] etc.

As a quasi-one-dimensional structure, graphene nanoribbon (GNR) can be formed by cutting the graphene along a typical direction. Due to the large fraction of carbon atoms on both edges, the electric property of GNR is somewhat different from that of the bulk graphene. There are two basic edge configurations of GNR, which are zigzag and armchair.[17] A finite-width GNR with general edge can be considered as a mixture of both zigzag GNR (ZGNR) and armchair GNR. Some earlier theoretical work has indicated that a ZGNR always shows metallic property due to the appearance of localized electronic states on the edge.[17–19] The edge state appears as a flat band at the Fermi level and contributes to a large density of states. Further investigation indicated that the ZGNR favors an antiferromagnetic ground state where an energy gap occurs at the Fermi level due to the edge magnetic moments.[17,20,21]

The experimental realization of GNR normally relies on lithographic,[3,11] chemical,[22–24] and synthetic[25] methods. In Ref. 24, the author demonstrated that the GNRs with width below 10 nm can been successfully manufactured with a chemical route.[24] More recently, a new method to fabricate the GNR was reported simultaneously by two groups with solution-based oxidative process[26] and Ar plasma etching method,[27] respectively, where GNR was realized by unzipping the multiwall armchair CNTs along the longitudinal direction. In Ref. 26, the ketones of unzipped edge of CNTs are converted into the carboxylic acids which align the edges of the GNR through O-protonated formations while the GNRs produced in Ref. 27 have bare edges. Within both methods, the unzipped degree of CNTs can be controlled through adjusting the experimental conditions, such as the amount of oxidizing agent introduced into the system.[26] Therefore, a nanotunneling junction is expected to be constructed based on the longitudinal unzipped CNTs. A theoretical investigation using the tight-binding (TB) model has been carried out to analyze the conductance of partly unzipped (6,6) CNT.[28]

In this paper, we carried out first-principles calculations to investigate the transport properties of unzipped carbon nanotube (UZCNT)-based tunneling junctions, where an infinite (4,4) CNT is unzipped in one lead or in a few unit cells in the central part. Specifically, five structures with different configurations and saturations at edges were investigated, which include two single junctions (4,4)CNT/8-ZGNR, (4,4)CNT/8-ZGNR-H (8 is the width of graphene nanoribbon and H stands for hydrogen saturation) and three double junctions (4,4)CNT/*N*-UZCNT-H/CNT (*N* stands for the number of unzipped unit cells), (4,4)CNT/*N*-UZCNT/CNT and (4,4)CNT/*N*-UZCNT-O/CNT. The conductances of (4,4)CNT/8-ZGNR calculated from *ab initio* method and TB model were compared and large difference was found. We concluded that accurate predictions of transport properties of this kind of hybrid structures have to rely on the *ab initio* calculations. We found that the (4,4)CNT/8-ZGNR-H structure possesses strongly spin-polarized transport properties due to the ferromagnetic configuration of magnetic moments on both edges of unzipped CNT. Importantly the (4,4)CNT/8-ZGNR-H magnetic tunneling junction (MTJ) can function as a spin filter. By changing the number *N* of unzipped unit cells, conductance of (4,4)CNT/*N*-UZCNT-H/CNT junction crossovers from CNT dominated to magnetic graphene dominated. When *N* is larger than 13, similar spin-filter property as that of (4,4)CNT/8-ZGNR-H MTJ was found. Finally, as a comparison, conductances of (4,4)CNT/*N*-UZCNT/CNT and (4,4)CNT/*N*-UZCNT-O/CNT were also calculated. We found that with increasing of *N*, systems change from perfect conductors to insulators.

II. STRUCTURE AND CALCULATION METHOD

The MTJs of (4,4)CNT/8-ZGNR-H and (4,4)CNT/20-UZCNT-H/CNT are schematically shown in Fig. 1. For

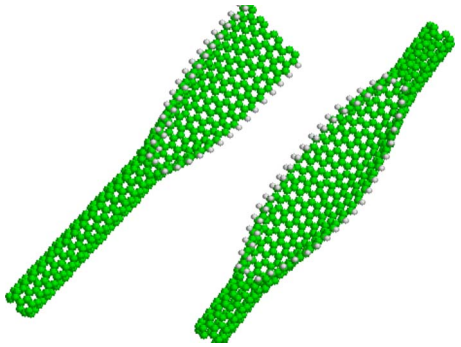

FIG. 1. (Color online) Schematic structures of (4,4)CNT/8-ZGNR-H MTJ and (4,4)CNT/20-UZCNT/CNT MTJ. The carbon atoms on the unzipped edges are irregularly saturated with hydrogen atoms.

single junctions (4,4)CNT/8-ZGNR and (4,4)CNT/8-ZGNR-H, one lead of an infinite (4,4) CNT was gradually unzipped to a perfect 8-ZGNR.[19] We assume that 17 unit cells are needed to gradually unfold a (4,4) CNT and form a perfect 8-ZGNR. For (4,4)CNT/8-ZGNR structure, the bonds at edges of unzipped part of CNT are unsaturated. But for (4,4)CNT/8-ZGNR-H structure, a special hydrogen-saturated configuration was considered where one edge of unzipped CNT was monohydrogenated and the other edge was dihydrogenated. Similar saturating technique has been implemented to ZGNR which has been shown to process finite magnetic moment.[12,29] This magnetic GNR is stable with robust magnetic moments.[29] We found that the (4,4)CNT/8-ZGNR-H structure also has finite magnetic moment and is therefore a MTJ. For the double junction (4,4)CNT/*N*-UZCNT-H/CNT, an infinite (4,4) CNT was unzipped at central part with *N* unzipped unit cells. The edges of unzipped part of CNT were also asymmetrically saturated with hydrogens similar to (4,4)CNT/8-ZGNR-H MTJ. For the junctions (4,4)CNT/*N*-UZCNT/CNT and (4,4)CNT/*N*-UZCNT-O/CNT, the bonds at edges of unzipped part of CNT are unsaturated and symmetrical monooxygenated saturated, respectively. For the latter structure, ketone groups are constructed at both edges of unzipped part of CNT. This structure is expected stable and has an antiferromagnetic ground state because the edge-ketonated ZGRN has been proved stable and has antiferromagnetic ground state.[30] For each junction, once the number of unzipped cells was fixed, its structure was obtained by total-energy relaxation using the SIESTA package.[31] A conjugate gradient method was used to achieve total-energy minimization until the residual force on each atom is less than 0.05 eV/Å. The relaxed bond length of the nearest C-H bond on the monohydrogenated edge, C-H bond on the dihydrogenated edge, and C-O bond are found to be 1.12, 1.136, and 1.243 Å, respectively.

To calculate spin-dependent transport properties, we carried out first-principles analysis of nonlinear spin-dependent quantum transport using a state-of-the-art atomistic technique based on density-functional theory (DFT) in combination with Keldysh nonequilibrium Green's functions (NEGF).[32,33] The basic principle and practical implementation of the NEGF-DFT formalism can be found in Ref. 34. In this method, system Hamiltonian as well as charge distribution are obtained from DFT calculation and nonequilibrium transport properties of the structure are determined by NEGF formalism. The self-consistent Hartree potential was obtained by solving the real-space Poisson equation. In our calculation, the exchange-correlation was treated at the local spin density approximation level[35] and a nonlocal pseudopotential developed by Troullier *et al.* was used.[36] Initial electronic density of states was constructed from linear combination of atomic orbital fireball basis set.[31] The NEGF-DFT self-consistency was controlled by a numerical tolerance of 10^{-4} eV.

The Hamiltonian of an open system with two leads can be divided into three parts: Hamiltonian of both leads H_α with $\alpha=L,R$, Hamiltonian of central device region H_c and the coupling between device and leads H_T as

$$H = H_\alpha + H_c + H_T. \tag{1}$$

Once the system Hamiltonian is obtained from the NEGF-DFT method, one can calculate the spin-dependent transmission coefficient $T_\sigma(E,V)$ as[37]

$$T_\sigma(E,V) = \mathrm{Tr}[\Gamma_L G^r \Gamma_R G^a]_{\sigma\sigma}, \tag{2}$$

where $\sigma=\pm 1$ $(\uparrow,\downarrow)$ and the trace is over the orbital space. Here G_r is the retarded Green's function defined as

$$G^r = \frac{1}{ES - H_c - \Sigma_L^r - \Sigma_R^r}. \tag{3}$$

In orbital space G^r is a $2n\times 2n$ matrix where the factor of 2 is due to spin and n is the number of the basis; S is the overlap matrix due to the nonorthogonal basis;[38,39] Σ^r is the self-energy describing the coupling between the pristine (4,4) CNT or 8-ZGNR and the unzipped segment; $i\Gamma_\alpha=\Sigma_\alpha^r-\Sigma_\alpha^a$.

At finite bias voltage, the spin-polarized current can be calculated using Landauer-Büttiker formula

$$I_\sigma(V) = \int_{-\infty}^{\infty} T_\sigma(E,V)[f(E-\mu_L) - f(E-\mu_R)]dE, \tag{4}$$

where f is the Fermi distribution function; $\mu_{L,R}$ are the chemical potentials of the left and right leads. In the zero-bias limit, spin-polarized conductance G_σ is obtained

$$G_\sigma = \frac{e^2}{h} T_\sigma(E_f), \tag{5}$$

where E_f is the Fermi energy. When spin is degenerate conductance G becomes

$$G = \frac{2e^2}{h} T(E_f). \tag{6}$$

III. RESULTS

Now we present numerical results. First, we calculated the conductance of (4,4)CNT/8-ZGNR junction using the TB model and then compared it with that of infinite (4,4) CNT and 8-ZGNR. In the TB model, we assume that the hopping

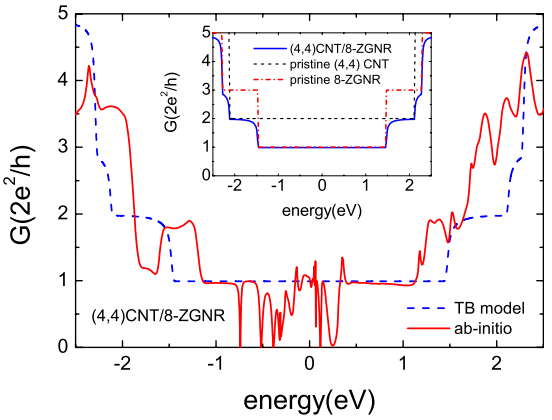

FIG. 2. (Color online) Comparison of conductances from TB model and *ab initio* calculation for (4,4)CNT/8-ZGNR junction. The blue dash line is from TB model and red real line is from *ab initio* calculation. Inset: conductances of pristine (4,4) CNT, pristine 8-ZGNR, and (4,4)CNT/8-ZGNR junction, which are indicated by black dash line, red dash-dot line, and blue real line, respectively.

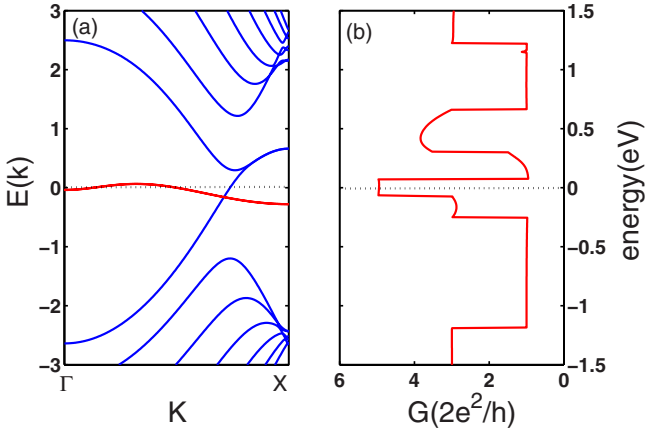

FIG. 3. (Color online) (a) Band structure of a periodic 8-ZGNR. (b) Transmission coefficient of the periodic 8-ZGNR.

energy t between carbon atoms in the unzipped CNT remains the same. Only π orbitals of carbon atoms were included with hopping energy $t=3$ eV. We have also neglected the spin polarization (SP) in this junction when using the TB model. As shown in the inset of Fig. 2, the transmission coefficient $T(E)$ of (4,4)CNT/8-ZGNR junction around $E=0$ is the same as that of the pristine 8-ZGNR. This is because the (4,4)CNT has higher symmetry whose $T(E)$ is two at the Fermi level than the pristine 8-ZGNR or the hybrid system (4,4)CNT/8-ZGNR junction. Therefore, the transport is dominated by the low-symmetry system 8-ZGNR in this energy range. When the energy increases to the range of [1.7, 2.1]eV, $T(E)$ becomes 2 and is equal to that of pristine (4,4) CNT. In this energy range, only two channels in CNT contribute to the electric transport although more channels are opened in the 8-ZGNR lead. Similar results for other CNT/ZGNR junctions have been reported in Ref. 28. Within the TB model, the transport properties of (4,4)CNT/8-ZGNR junction are simple and intuitive. However, accurate description of transport properties of (4,4)CNT/8-ZGNR junction must come from first-principles calculation. As shown in Fig. 2, conductance from first principles is completely different from that of the TB model. In particular, around $E=0$, G is very sensitive to the energy and at certain energies a complete reflection occurs indicating the existence of antiresonant states. In addition, it is find that G can be larger than 1 around the Fermi level. It can be understood as follows. For a periodic 8-ZGNR without edge saturation, a double-degenerate flat band will appears around the Fermi level due to the dangling bonds at both edge, which contribute to the transmission coefficient. Figure 3(a) shows the band structure of 8-ZGNR and Fig. 3(b) shows the conductance G of a periodic 8-ZGNR. We can find that a double-degenerate state appears around the Fermi level in Fig. 3(a) and the corresponding transmission coefficient can reach to 5 as shown in Fig. 3(b). This is very different from that obtained in TB model, where there is only one channel around the Fermi level and maximum value of transmission coefficient is 1. From now on, we shall only present *ab initio* investigations on transport properties of these systems.

The second device we considered is the (4,4)CNT/8-ZGNR-H junction. Due to the asymmetrical saturation of hydrogen atoms on the unzipped edges, we found that (4,4)CNT/8-ZGNR-H structure processes finite magnetic moment showing strongly spin-polarized transport properties. As a result, this structure can be regarded as a MTJ and can function as a spin filter. Figure 4 shows the spin-polarized conductance of the (4,4)CNT/8-ZGNR-H MTJ. For comparison, the conductances of pristine (4,4) CNT as well as pristine 8-ZGNR-H calculated from first principle are also presented. In this figure, the upper half panel represents the spin-up channel while the lower half panel is for the spin-down channel. For the pristine 8-ZGNR-H structure, a small gap appears for both the spin-up and spin-down channels around the Fermi level $E=0$. This can be understood by considering the entirely spin-polarized localized states as shown in the insets of Fig. 4, where a nearly flat band is below (above) the Fermi level for spin-up (-down) channels.[12,29] Each of these two flat bands contributes a spin-

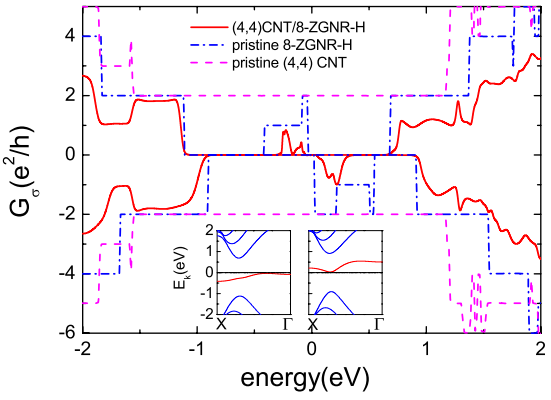

FIG. 4. (Color online) Spin-polarized dc conductances of (4,4)CNT/8-ZGNR-H MTJ, pristine (4,4) CNT, and 8-ZGNR-H. The upper half panel indicates the spin-up branch and lower half panel indicates the spin-down branch. Inset: band structures of pristine 8-ZGNR-H for spin-up channels (left panel) and spin-down channels (right panel).

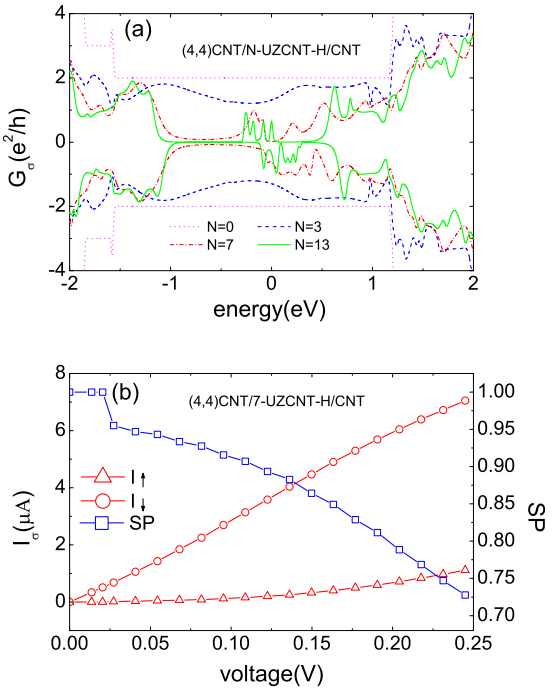

FIG. 5. (Color online) (a) Spin-polarized dc conductance versus the energy for (4,4)CNT/*N*-UZCNT-H/CNT MTJ. The pink dot line, blue dash line, red dot-dash line, and green real line correspond to $N=0$, 3, 7, and 13, respectively, where $N=0$ means a pristine (4,4) CNT. (b) Spin-polarized charge current and spin polarization versus the bias voltage for (4,4)CNT/7-UZCNT-H/CNT MTJ. The red triangle line and red circle line indicate $I_\uparrow$ and $I_\downarrow$, respectively, and the blue square line indicates the SP.

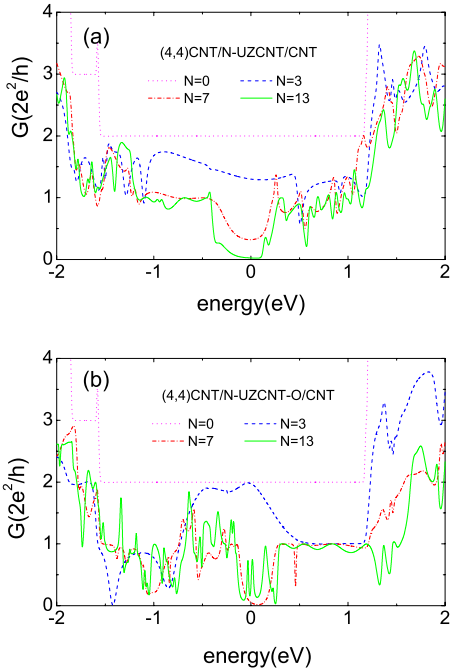

FIG. 6. (Color online) dc conductance versus energy for (a) (4,4)CNT/*N*-UZCNT/CNT structure and (b) (4,4)CNT/*N*-UZCNT-O/CNT structure. The pink dot line, blue dash line, red dot-dash line, and green real line correspond to $N=0$, 3, 7, and 13, respectively.

dependent transmission coefficient with $T(E)=1$ or 2 around the Fermi level. For the (4,4)CNT/8-ZGNR-H MTJ, the conductance also shows the spin-polarized properties. Due to the hybridization (4,4) CNT and 8-ZGNR-H the gap near the Fermi level $E=0$ becomes wider and the system is an insulator in this energy range.

When energy is between $E=(0.05,0.33)$ eV, $G_\downarrow$ is nonzero and (4,4)CNT/8-ZGNR-H MTJ becomes a half metal allowing only spin-down electrons. When $E=(0.33,0.68)$ the system is an insulator. This behavior is understandable in the energy range $E=(0.55,0.68)$ since the 8-ZGNR-H lead is an insulator. It is interesting to see that although both (4,4)CNT and 8-ZGNR-H are in the metallic regime in $E=(0.33,0.55)$, the hybrid system becomes an insulator. This could be due to the decrease in the flat bandwidth of the curved 8-ZGNR-H. When energy increases further from 0.68 to 0.91 eV, a finite $G_\uparrow$ appears with $G_\downarrow$ still equal to zero. In this energy range, system changes to a perfect spin-down filter. When energy is decreased from zero to a negative value, spin-filtering properties are similar to that in the positive-energy range. Obviously, (4,4)CNT/8-ZGNR-H MTJ can serve as different kind of spin filters by energy variations. With the increase in energy from 0 to 0.85 eV, the system is expected to transform from an insulator to a spin-down half metal, then to an insulator again and finally a spin-up half metal.

As the third example, we investigated the double junction (4,4)CNT/*N*-UZCNT-H/CNT by changing the number of unzipped CNT unit cell denoted as *N*. $G_\uparrow$ and $G_\downarrow$ are depicted in Fig. 5(a) where the upper half panel shows the spin-up branch and lower half panel is for the spin-down branch. When $N=3$, $G_\uparrow$ and $G_\downarrow$ are slightly smaller than that of pristine (4,4) CNT. When $N=7$, the conductance decreases significantly and the spin-polarized properties are manifest. An energy gap occurs for the spin-up channel at the Fermi level. When $N=13$, the conductance is very similar to that of (4,4)CNT/8-ZGNR-H MTJ except that more features appear around the Fermi level. Therefore, we expect that similar spin-filtering properties can be found in (4,4)CNT/*N*-UZCNT-H/CNT MTJs with *N* larger than 13. We also calculated the *I*-*V* curve of (4,4)CNT/7-UZCNT-H/CNT MTJ as shown in Fig. 5(b). With the increase in bias voltage from 0 to 0.25 V, $I_\downarrow$ is always larger than $I_\uparrow$. This is understandable from Fig. 5(a) since the transmission coefficient of spin-down electron is always larger than that of spin-up electron. In particular, when voltage is lower than 0.02 V, only the spin-down electron can pass through the system and the system is a perfect spin-down half metal. In order to describe the variation in spin-polarized current, we introduce SP as

$$\mathrm{SP}=\frac{I_\downarrow-I_\uparrow}{I_\downarrow+I_\uparrow}. \tag{7}$$

Under the zero-bias voltage, $I_\uparrow$ ($I_\downarrow$) is replaced by $G_\uparrow$ ($G_\downarrow$). For (4,4)CNT/7-UZCNT-H/CNT MTJ, the spin polarization is one from 0 to 0.02 V and then decreases to 0.725 at $V=0.25$ V.

Finally, we also investigated the conductance of (4,4)CNT/*N*-UZCNT/CNT structure where the bonds at

edges are unsaturated and (4,4)CNT/*N*-UZCNT-O/CNT structure where both edges are symmetrical monooxygenated saturated. These two structures are relaxed to antiferromagnetic ground states. Figure 6 shows their conductances with different *N*. We see that with the increase in *N*, conductance decreases and finally shows a large gap at the Fermi level. This can be understood by examining the energy gap at the Fermi level of periodic 8-ZGNR and 8-ZGNR-O structures in the antiferromagnetic ground states. The larger the *N* is, the more similar the unzipped CNT is to the ZGNR. Therefore, we expect that when *N* is larger than 13, the properties of (4,4)CNT/*N*-UZCNT/CNT and (4,4)CNT/*N*-UZCNT-O/CNT structures are mostly dominated by the ZGNR rather than the CNT.

In summary, we have investigated the spin-dependent transport properties of unzipped (4,4) CNT based MTJs. Under a special edge-saturated configuration, where one edge of unzipped CNT is monohydrogenated and the other edge is dihydrogenated, (4,4)CNT/8-ZGNR-H MTJ functions as a spin filter. With the increase in the Fermi level from 0 to 0.85 eV, the system changes from an insulator to a spin-down half metal, then to an insulator again and finally a spin-up half metal. Similar properties were found for the (4,4)CNT/*N*-UZCNT-H/CNT structure with *N* larger than 13. Conductances of (4,4)CNT/*N*-UZCNT/CNT and (4,4)CNT/*N*-UZCNT-O/CNT structures show that these systems change from a conductor to an insulator near the Fermi level with the increase in unzipped number *N*.

ACKNOWLEDGMENTS

We thank W. Ren for useful discussion. We gratefully acknowledge the financial support by a RGC (Grant No. HKU 704308P) from the government of HKSAR.

*jianwang@hkusub.hku.hk

[1] K. S. Novoselov, A. K. Geim, S. V. Morozov, D. Jiang, Y. Zhang, S. V. Dubonos, I. V. Grigorieva, and A. A. Firsov, Science **306**, 666 (2004).
[2] K. S. Novoselov, A. K. Geim, S. V. Morozov, D. Jiang, M. I. Katsnelson, I. V. Grigorieva, S. V. Dubonos, and A. A. Firsov, Nature (London) **438**, 197 (2005).
[3] Y. Zhang, Y. W. Tan, H. L. Stormer, and P. Kim, Nature (London) **438**, 201 (2005).
[4] C. L. Kane and E. J. Mele, Phys. Rev. Lett. **95**, 226801 (2005).
[5] H. Min, J. E. Hill, N. A. Sinitsyn, B. R. Sahu, L. Kleinman, and A. H. MacDonald, Phys. Rev. B **74**, 165310 (2006).
[6] N. A. Sinitsyn, J. E. Hill, H. Min, J. Sinova, and A. H. MacDonald, Phys. Rev. Lett. **97**, 106804 (2006).
[7] D. A. Abanin, P. A. Lee, and L. S. Levitov, Phys. Rev. Lett. **96**, 176803 (2006).
[8] Z. H. Qiao, J. Wang, Y. D. Wei, and H. Guo, Phys. Rev. Lett. **101**, 016804 (2008).
[9] F. Miao, S. Wijeratne, Y. Zhang, U. C. Coskun, W. Bao, and C. N. Lau, Science **317**, 1530 (2007).
[10] Y.-W. Son, M. L. Cohen, and S. G. Louie, Nature (London) **444**, 347 (2006).
[11] M. Y. Han, B. Ozyilmaz, Y. Zhang, and P. Kim, Phys. Rev. Lett. **98**, 206805 (2007).
[12] B. Wang, J. Wang, and H. Guo, Phys. Rev. B **79**, 165417 (2009).
[13] V. V. Cheianov and V. I. Fal'ko, Phys. Rev. B **74**, 041403(R) (2006).
[14] W. Long, Q. F. Sun, and J. Wang, Phys. Rev. Lett. **101**, 166806 (2008).
[15] J. Li and S. Q. Shen, Phys. Rev. B **78**, 205308 (2008).
[16] T. G. Pedersen, C. Flindt, J. Pedersen, N. A. Mortensen, A. P. Jauho, and K. Pedersen, Phys. Rev. Lett. **100**, 136804 (2008).
[17] M. Fujita, K. Wakabayashi, K. Nakada, and K. Kusakabe, J. Phys. Soc. Jpn. **65**, 1920 (1996).
[18] S. E. Stein and R. L. Brown, J. Am. Chem. Soc. **109**, 3721 (1987).
[19] K. Nakada, M. Fujita, G. Dresselhaus, and M. S. Dresselhaus, Phys. Rev. B **54**, 17954 (1996).
[20] A. Yamashiro, Y. Shimoi, K. Harigaya, and K. Wakabayashi, Phys. Rev. B **68**, 193410 (2003).
[21] H. Lee, Y.-W. Son, N. Park, S. Han, and J. Yu, Phys. Rev. B **72**, 174431 (2005).
[22] S. Stankovich, R. D. Piner, S. T. Nguyen, and R. S. Ruoff, Carbon **44**, 3342 (2006).
[23] H. C. Schniepp, J. L. Li, M. J. McAllister, H. Sai, M. H. Alonso, D. H. Adamson, R. K. Prud'homme, R. Car, D. A. Saville, and I. A. Aksay, J. Phys. Chem. B **110**, 8535 (2006).
[24] X. Li, X. Wang, L. Zhang, S. Lee, and H. J. Dai, Science **319**, 1229 (2008).
[25] X. Yang, X. Dou, A. Rouhanipour, L. Zhi, H. J. Räder, and K. Müllen, J. Am. Chem. Soc. **130**, 4216 (2008).
[26] D. V. Kosynkin, A. L. Higginbotham, A. Sinitskii, J. R. Lomeda, A. Dimiev, B. K. Price1, and J. M. Tour, Nature (London) **458**, 872 (2009).
[27] L. Jiao, L. Zhang, X. Wang, G. Diankov, and H. J. Dai, Nature (London) **458**, 877 (2009).
[28] H. Santos, L. Chico, and L. Brey, Phys. Rev. Lett. **103**, 086801 (2009).
[29] K. Kusakabe and M. Maruyama, Phys. Rev. B **67**, 092406 (2003).
[30] O. Hod, V. Barone, J. E. Peralta, and G. E. Scuseria, Nano Lett. **7**, 2295 (2007).
[31] P. Ordejón, E. Artacho, and J. M. Soler, Phys. Rev. B **53**, R10441 (1996); J. M. Soler, E. Artacho, J. D. Gale, A. García, J. Junquera, P. Ordejón, and D. Sánchez-Portal, J. Phys.: Condens. Matter **14**, 2745 (2002).
[32] D. Waldron, P. Haney, B. Larade, A. MacDonald, and H. Guo, Phys. Rev. Lett. **96**, 166804 (2006).
[33] D. Waldron, V. Timoshevskii, Y. Hu, K. Xia, and H. Guo, Phys. Rev. Lett. **97**, 226802 (2006).
[34] J. Taylor, H. Guo, and J. Wang, Phys. Rev. B **63** 245407 (2001); **63** 121104 (2001).
[35] U. von Barth and L. Hedin, J. Phys. C **5**, 1629 (1972); O. Gunnarsson and B. I. Lundqvist, Phys. Rev. B **13**, 4274 (1976); A. K. Rajagopal, J. Phys. C **11**, L943 (1978).
[36] N. Troullier and J. L. Martins, Phys. Rev. B **43**, 1993 (1991).

[37] B. G. Wang, J. Wang, and H. Guo, J. Phys. Soc. Jpn. **70**, 2645 (2001).
[38] K. S. Thygesen, Phys. Rev. B **73**, 035309 (2006).
[39] For dc transport it can be shown that the values of transmission coefficient are the same regardless whether the orbitals are orthogonal or nonorthogonal. In ac transport, however, the current expression derived from the orthogonal basis set can not be used for nonorthogonal basis.